Title

Two-Dimensional Copper Iodide-Based Inorganic–Organic Hybrid Semiconductors: Synthesis, Structures, and Optical and Transport Properties

Journal

Chemistry of Materials, 33(13)

ISSN

0897-4756

Authors

Ki, Wooseok
Hei, Xiuze
Yi, Hee Taek
et al.

Publication Date

2021-07-13

DOI

10.1021/acs.chemmater.1c01421

Peer reviewed

Two-Dimensional Copper Iodide Based Inorganic-Organic Hybrid Semiconductors: Synthesis, Structures, Optical and Transport Properties

Wooseok Ki,[a,b,+] Xiuze Hei,[a,+] Hee Taek Yi,[c] Wei Liu,[a,d] Simon J. Teat,[e] Mengjun Li,[a] Yang Fang,[a] Vitaly Podzorov,[c] Eric Garfunkel[a] and Jing Li[a,*]

[a] Department of Chemistry and Chemical Biology, Rutgers University, 123 Bevier Road, Piscataway, New Jersey 08854, USA

[b] School of Natural Sciences and Mathematics, Stockton University, 101 Vera King Farris Drive, Galloway, NJ 08205 USA

[c] Department of Physics and Astronomy, Rutgers University, 136 Frelinghuysen Road, Piscataway, NJ 08854, USA

[d] Hoffman Institute of Advanced Materials, Shenzhen Polytechnic, 7098 Liuxian Bl, Nanshan District, Shenzhen, 518055, China

[e] Advanced Light Source, Lawrence Berkeley National Laboratory, 1 Cyclotron Road, Berkeley, CA 94720, USA

[+] Equal contributions

Corresponding author: jingli@rutgers.edu

Abstract: A group of copper iodide based hybrid semiconductors with the general formula of 2D-CuI(L)$_{0.5}$ (L = organic ligands) are synthesized and structurally characterized. All compounds are two-dimensional (2D) networks made of one-dimensional (1D) copper iodide staircase chains that are interconnected by bidentate Nitrogen containing ligands. Results from optical absorption and emission experiments and density functional theory (DFT) calculations reveal that their photoluminescence (PL) can be systematically tuned by adjusting the lowest unoccupied molecular orbital (LUMO) energies of the organic ligands. Charge carrier transport measurements were carried out for the first time on single crystals of selected 2D-CuI(L)$_{0.5}$ structures and the results show that they possess p-type conductivity with a Hall mobility of ~ 1 $cm^2V^{-1}s^{-1}$ for 2D-CuI(pm)$_{0.5}$ and 0.13 $cm^2V^{-1}s^{-1}$ for 2D-CuI(pz)$_{0.5}$, respectively. These values are comparable to or higher than the mobilities of typical highly luminescent organic semiconductors. This work suggests that robust, high-dimensional copper iodide hybrid semiconductors are promising candidates to be considered as a new type of emissive layers for LED devices.

Introduction

While high-performance photoluminescent (PL) materials are very important for general lighting applications, there has also been an increasing demand for highly efficient electroluminescent (EL) materials for use in full-color, light-weight and flexible displays as well as various LED devices.[1-2] Either poor charge transport or low luminescence efficiency remain to be the two main challenges for organic semiconductors currently used in organic light-emitting diodes (OLEDs). For example, strongly emissive organic materials such as tris(8-hydroxy quinoline) aluminum (Alq_3) or phenylenevinylene-based polymers show poor charge transport with low carrier mobilities (10^{-6}-10^{-5} $cm^2V^{-1}s^{-1}$);[3-4] On the other hand, high mobility (> 1 $cm^2V^{-1}s^{-1}$) organic semiconductors typically exhibit very low luminescence quantum efficiency, because of their aggregation-induced quenching.[5-7] Conversion of short-lived singlet excitons to long-lived triplets via the intersystem crossing in rare-earth element (REE) containing organic molecules, such as Ir or Eu based complexes, has proven to be an effective approach for improving the device efficiency, but these elements are very costly.[8-9] In addition, thermal evaporation under high vacuum is typically used for the fabrication of small molecule based active layers in OLEDs, which suffers from low throughput and high cost.[10-11] Therefore, developing highly luminescent, low-cost, solution-processable semiconductors with tunable band gaps and relatively high charge carrier mobilities represents a major leap forward in the future development of light-emitting-diode (LED) technologies.

Copper iodide based crystalline inorganic-organic hybrid materials have attracted great attention in the recent years due to their structural diversity and unique optical properties, which demonstrate strong potential for general lighting related applications.[12-21] Several types of structures with different inorganic building motifs have been developed, and intensive studies have been carried out to improve their optical properties and chemical/thermal stability.[22-23] However, investigation of their electric properties as EL materials remains underexplored. Among numerous types of structures, those that are built of one-dimensional (1D) CuI chains are of particular interest, as the infinite chains of the inorganic motif may act as a highly efficient pathway for charge transport, thereby generating high carrier mobility required for good EL materials, and the organic ligands in these structures would be largely responsible for their optical tunability.[24-28]

To test out the above hypothesis, we synthesized a series of 2D-CuI(L)$_{0.5}$ compounds containing infinite 1D chains of copper iodide. Bidentate ligands, including bipyridine, pyrazine, pyrimidine, imidazole, triazole and their derivatives were used for the construction these 2D network structures with the neighboring chains interconnected by the ligands. All structures have the formula 2D-CuI(L)$_{0.5}$, where L is a bidentate ligand. Large millimeter-sized single crystals of 2D-CuI(pm)$_{0.5}$ and 2D-CuI(pz)$_{0.5}$ were obtained by slow diffusion growth method and were used for electric property studies. Results

from Hall Effect measurements indicate that they have high charge carrier mobilities (up to ~1 $cm^2V^{-1}s^{-1}$), which are significantly higher than those of typical highly luminescent organic semiconductors.

Experimental

Materials.

CuI (98 %, Alfa Aesar), acetonitrile (ACN, >99%, Alfa Aesar), pyrimidine (*pm*, 98 %, Alfa Aesar), pyrazine (*pz*, 98 %, Alfa Aesar), 1,2-bis(4-pyridyl)ethane (*bpe*, 99 %, Sigma Aldrich), 1,2-bis(4-pyridyl)ethylene (*bpee*, 97 %, Sigma Aldrich), 4,4'-bipyridyl (*4,4'-bpy*, >98.0 %, TCI), 1,4-bis(bromomethyl)benzene (97 %, Alfa Aesar), benzimidazole (99%, Alfa Aesar), dimethyl sulfoxide (DMSO, >99%, Alfa Aesar), NaOH (98%, Alfa Aesar) sodium salicylate (99 %, Merck), YAG:Ce^{3+}type 9800 (Global Tungsten & Powders Corp), KI (99 %, Alfa Aesar). All chemicals were used as received without further purifications.

Synthesis of 1,4-bis((1H-benzo[d]imidazol-1-yl)methyl)benzene (*bbimb*).

1.2 g (30 mmol) NaOH was added to a solution of 1.18 g (10 mmol) benzimidazole in 20 ml DMSO. The mixture was stirred at 70 °C for 2 hours, followed by injection of 540 µl (4 mmol) 1,4-bis(bromomethyl)benzene into the solution. The reaction mixture was heated at 100 °C overnight. After cooling to room temperaturethe solution was then poured into 150 ml cold water for 3 hours. The solution was extracted with methylene chloride three times, and the combined extraction were concentrated in vacuum to white solid. Pure product of *bbimb* in high yield (80 %) was obtained after recrystallization with acetone/hexane (v:v = 1:1) solution.

General Synthesis Procedures of compounds 1-6.

Single crystals of 2D-CuI$(pm)_{0.5}$ (**1**), 2D-CuI$(pz)_{0.5}$ (**2**), 2D-CuI$(4,4'\text{-}bpy)_{0.5}$ (**3**), 2D-CuI$(bpe)_{0.5}$ (**4**), 2D-CuI$(bpee)_{0.5}$ (**5**), 2D-CuI$(bbimb)_{0.5}$ (**6**) were acquired by slow diffusion method.[29] The reactions were conducted in glass vials at room temperature. The bottom, middle and top layers were CuI/KI saturated aqueous solution, acetonitrile, and ligand in ethanol, respectively. The crystals formed in the middle layer over 3-5 days at room temperature. Pure phase powder samples were obtained by direct mixing of CuI (0.019 g, 0.1 mmol) in saturated KI solution with ligand (0.1mmol) in ethanol. The ligand solution was added dropwise to prevent the formation of different phases. The pure phase powder generally formed immediately after stirring. Mild heating at 60 °C overnight may be helpful for obtaining samples of higher crystallinity. Larger single crystal growth for electric measurements were obtained by similar method under optimized conditions.

Synthesis of compound 1.

CuI (0.19 g, 1 mmol) was first dissolved in KI saturated solution (2 ml) in a reaction vial. Acetonitrile (2 ml) was added as another layer and then *pm* (1 mmol) in methanol (2 ml) was added slowly into the vial. The reaction mixture was kept undisturbed at room temperature, and plate-shaped single crystals formed in 3 days and were collected by filtration. Yield is 45%. Millimeter-sized single crystals of 2D-CuI(pm)$_{0.5}$ was grown by a modified diffusion growth method. A solution of CuI (0.19 g, 1.0 mmol) in saturated potassium iodide (KI) solution (2.0 mL) and a solution of 0.5 mmol *pm* in ethanol (2.0 mL) were separated by a layer of 2.0 mL of acetonitrile used as a middle layer. The solution was then placed into oven at 60 ºC for 1 day, which is necessary to grow large and thin plate crystals.

Synthesis of compound 2.

Acetonitrile (2 ml) was added into KI saturated solution (2 ml) containing CuI (0.19 g, 1 mmol), and then *pz* (1 mmol) in methanol (2ml) was slowly added. Plate-shaped single crystals formed in one day and were collected by filtration. Yield is 60%. The mm-sized single crystal was synthesized as same as compound **1**.

Synthesis of compound 3.

CuI (0.19 g, 1 mmol) was first dissolved in KI saturated solution (2 ml) in a reaction vial. Acetonitrile (2 ml) was added as another layer and then *4.4'-bpy* (1 mmol) in methanol (2 ml) was added slowly into the vial. The reaction mixture was kept undisturbed at room temperature, and plate-shaped single crystals formed in 3 days and were collected by filtration. Yield is 45%.

Synthesis of compound 4.

Acetonitrile (2 ml) was added into KI saturated solution (2 ml) containing CuI (0.19 g, 1 mmol), and then *bpe* (1 mmol) in methanol (2ml) was slowly added. Plate-shaped single crystals formed in one day and were collected by filtration. Yield is 60%.

Synthesis of compound 5.

CuI (0.19 g, 1 mmol) was first dissolved in KI saturated solution (2 ml) in a reaction vial. Acetonitrile (2 ml) was added and then *bpee* (1 mmol) in methanol (2 ml) was added slowly in to the vial. The reaction mixture was kept at 60 ºC for 1 day, orange crystalline powder formed was collected by filtration. Yield is 75%.

Synthesis of compound 6.

CuI (0.19 g, 1 mmol) was first dissolved in KI saturated solution (2 ml) in a reaction vial. Acetonitrile (2 ml) was added and then *bbimb* (1mmol) in methanol (2 ml) was added slowly in to the vial. The reaction mixture was

kept at 60 °C for 1 day, and the crystalline powder was collected by filtration. Yield is 55%.

Single crystal X-ray diffraction (SXRD) and Powder X-ray diffraction (PXRD) analysis.

Single crystal diffraction data were collected using a D8 goniostat equipped with a Bruker PHOTON100 CMOS detector using synchrotron radiation at the Advanced Light Source (ALS), Lawrence Berkeley National Laboratory. The refinement method used was full-matrix least squares on F^2. CCDC numbers are: 2005656 and 2077521. Powder X-ray diffraction (PXRD) analyses were carried out on a Rigaku Ultima-IV unit using Cu Kα radiation (λ = 1.5406 Å). The data were collected at room temperature in a 2θ range of 3-40° with a scan speed of 2°/min. The operating power was 40 kV/40 mA.

Thermogravimetric analysis.

Thermogravimetric analyses (TGA) were performed on powder samples using the TA Instrument Q5000IR thermal gravimetric analyzer with nitrogen flow and sample purge rate at 10 ml/min and 12 ml/min respectively. About 1-3 mg of samples were loaded onto a platinum sample pan and heated from room temperature to 450 °C at a rate of 10 °C/min under nitrogen flow.

Optical measurements.

Optical absorption spectra were measured at room temperature on a Shimadzu UV-3600 UV/VIS/NIR spectrometer. The reflectance data were converted to Kubelka-Munk function, $\alpha/S = (1-R)^2/2R$ (α is absorption coefficient, S is scattering coefficient and R is reflectance), and used to estimate the bandgap. The scattering coefficient (S) was treated as a constant as the average particle size of the samples used in the measurements was significantly larger than 5 μm. Samples for optical reflectance measurements were prepared by evenly distributing ground powders between two quartz slides. Photoluminescence (PL) measurements were carried out on a Varian Cary Eclipse spectrophotometer at room temperature. Powder samples were evenly distributed and sandwiched between two glass slides (which do not have emission in the visible range) for all measurements. Internal quantum yield (IQY) of samples in powder form was measured on a C9920-03 absolute quantum yield measurement system (Hamamatsu Photonics) with a 150 W xenon monochromatic light source and 3.3 inch integrating sphere. Sodium salicylate and YAG:Ce^{3+} were chosen as the standards with an IQY of 60% and 95% at 360 nm and 455 nm, respectively.[30-31] Their IQY values were measured to be 66% and 99%, respectively which were used to calibrate the values obtained on other samples.

Scanning Kelvin probe microsope (SKPM) measurements.

These experiments were conducted on Park Systems model NX-10 AFM with EFM mode. The tip used was NSC14/CR-AU from MikroMasch. The energy resolution was ~10 meV and the spatial resolution was ~30 nm. Highly oriented pyrolytic graphite (HOPG) was used as the reference and its surface potentials before and after measurements of the samples display consistent value, confirming the tip stays in the same condition when measuring the samples. UPS experiment was then performed on HOPG to obtain its absolute work function, which was estimated to be 5.5 eV. The potential difference between HOPG and the tip was around 8 mV. Considering the resolution of the KPM, the intrinsic potential was calculated to be 5.50 V. The average potential differences of 2D-Cu(pm)$_{0.5}$ and 2D-Cu(pz)$_{0.5}$ were then measured to be -34 mV and -24 mV, respectively. As a result, the work function of 2D-Cu(pm)$_{0.5}$ and 2D-Cu(pz)$_{0.5}$ were determined to be 5.46 eV and 5.26 eV, respectively.

Hall effect measurements.

Prior to the Hall effect measurements, single crystals were sonicated in isopropyl alcohol for 5 seconds to clean the surface. Electrical contacts were painted on top of the crystals with an aqueous solution of colloidal graphite (Ted Pella) and contacted with 25-μm thick gold wires. Hall measurements were performed at room temperature in air. We used a DL1201 voltage preamplifier (DL Instruments) and a Stanford Research SR-830 lock-in amplifier for Hall voltage measurements, Keithley current source K6221 for ISD excitation, and Electrometer K6514 for four-probe voltage measurements. An ac magnetic field of a frequency 0.6–2 Hz with a root-mean-square magnitude of Brms = 0.23 T was generated by rotating an assembly of strong permanent Nd magnets fixed on an Al frame.

Results and Discussion

Crystal growth and structures.

Various approaches have been developed to grow single crystals of copper halide based hybrid structures. Among them, slow diffusion is one of the most efficient methods for obtaining high quality crystals of chain type structures. Because of the fast nucleation rate, these compounds generally precipitate out immediately after direct mixing of the copper iodide with the ligands at room temperature. To slow down the reaction and to promote crystallization process, a third solvent, namely acetonitrile, was used in our synthesis as a buffer layer and was placed between two solutions containing copper iodide (CuI/KI aqueous solution) and ligand (methanol solution). With this approach, we obtained high quality crystal samples of six compounds: 2D-CuI(pm)$_{0.5}$ (**1**), 2D-CuI(pz)$_{0.5}$ (**2**), 2D-CuI(*4,4'-bpy*)$_{0.5}$ (**3**), 2D-CuI(bpe)$_{0.5}$ (**4**), 2D-CuI($bpee$)$_{0.5}$ (**5**) and 2D-CuI($bbimb$)$_{0.5}$ (**6**). Compounds **3** and **6** are new structures and their crystallographic data are summarized in Table 1. Powder samples of these compounds could be obtained by directly mixing the

ligands with CuI/KI solution, and their phase purity has been confirmed by PXRD analysis (Fig. S2). It is worth mentioning that the amount of ligands used has notable influence on the final product. The targeted 2D-CuI$(L)_{0.5}$ structures would form preferably under ligand-deficient conditions, so ligands must be added slowly into the CuI solution with controlled amount in order to avoid the formation of other types of structures. Adding ligand quickly or in excess amount might lead to the formation of Cu_2I_2 dimer-based structures.

Table 1. Summary of crystal data of new 2D-CuI$(L)_{0.5}$ structures

Compound	**2D-CuI(*bpe*)$_{0.5}$ (3)**	**2D-CuI(*bbimb*)$_{0.5}$ (6)**
Crystal System	triclinic	monoclinic
Empirical Formula	C_6H_6CuIN	$C_{11}H_9CuIN_2$
FW	282.56	359.64
Space Group	P-1	$P2_1/c$
a (Å)	4.2051(4)	4.4331(2)
b (Å)	9.0869(8)	16.9180(6)
c (Å)	10.1661(8)	13.7095(5)
α (°)	102.183(5)	90
β (°)	95.680(6)	97.495(2)
γ(°)	97.483(6)	90
V (Å^3)	373.26(6)	1019.42(7)
Z	2	4
T (K)	298(2)	100(2)
λ(Å)	0.7749	0.7749
R_1	0.0319(1437)	0.0172(3696)
wR_2	0.0718(1632)	0.0425(3874)

All six structures are composed of staircase chains of 1D-CuI linked by bidendate ligands, giving rise to an overall 2D network (Fig. S1). A

typical structure is shown in Figure 1. By varying the length of the bridging ligand, the separation between adjacent CuI chains can be easily controlled (Table 2), which is from 5.75 Å to 14.77 Å, measured as the distance between the two closest copper atoms from two adjacent chains. The distances between the adjacent sheets vary from 7.02 to 10.38 Å and are also summarized in Table 2. It is worth noting that the distances between the adjacent ligands range from 3.40 to 3.77 Å, well within the length scale of π-π interactions. Such interactions may also contribute to the mobility.[32]

Table 2. Inter-chain and inter-layer distances in 2D-CuI(L)$_{0.5}$

Compound	Inter-chain (Å)	Inter-layer (Å)	Ligand π-π distance (Å)
2D-CuI(*pm*)$_{0.5}$	5.75	7.02	3.66
2D-CuI(*pz*)$_{0.5}$	6.86	6.25	3.56
2D-CuI(*4,4'-*	11.19	8.14	3.62
2D-CuI(*bpe*)$_{0.5}$	13.45	8.31	3.77
2D-CuI(*bpee*)$_{0.5}$	13.51	8.30	3.60
2D-CuI(*bbimb*)$_{0.5}$	14.77	9.23	3.40

Optical Properties.

The optical absorption spectra of compounds **1**-**6** were recorded at room temperature and converted to the Kubelka-Munk function. The band gaps were estimated from their absorption edges. The values are 2.5, 2.25, 2.3, 3.1, 2.2, and 2.35 eV, respectively, for **1**-**6** (see Figure 2a and Table 3). This trend correlates well with that of the LUMO energies of the organic ligands in the structures (see Table S1). As shown in Figure 2b and Table 3, except compound **6**, other structures all emit in the visible light region and their emission colors range from purple to red. Their emission profiles are all single-band type, with an average of full width at half maximum (FWHM) of ~100 nm. The emission energies of these compounds are also in trend with their band gaps and the LUMO energies of the corresponding ligands. Their excitation spectra can be found in Fig. S3.

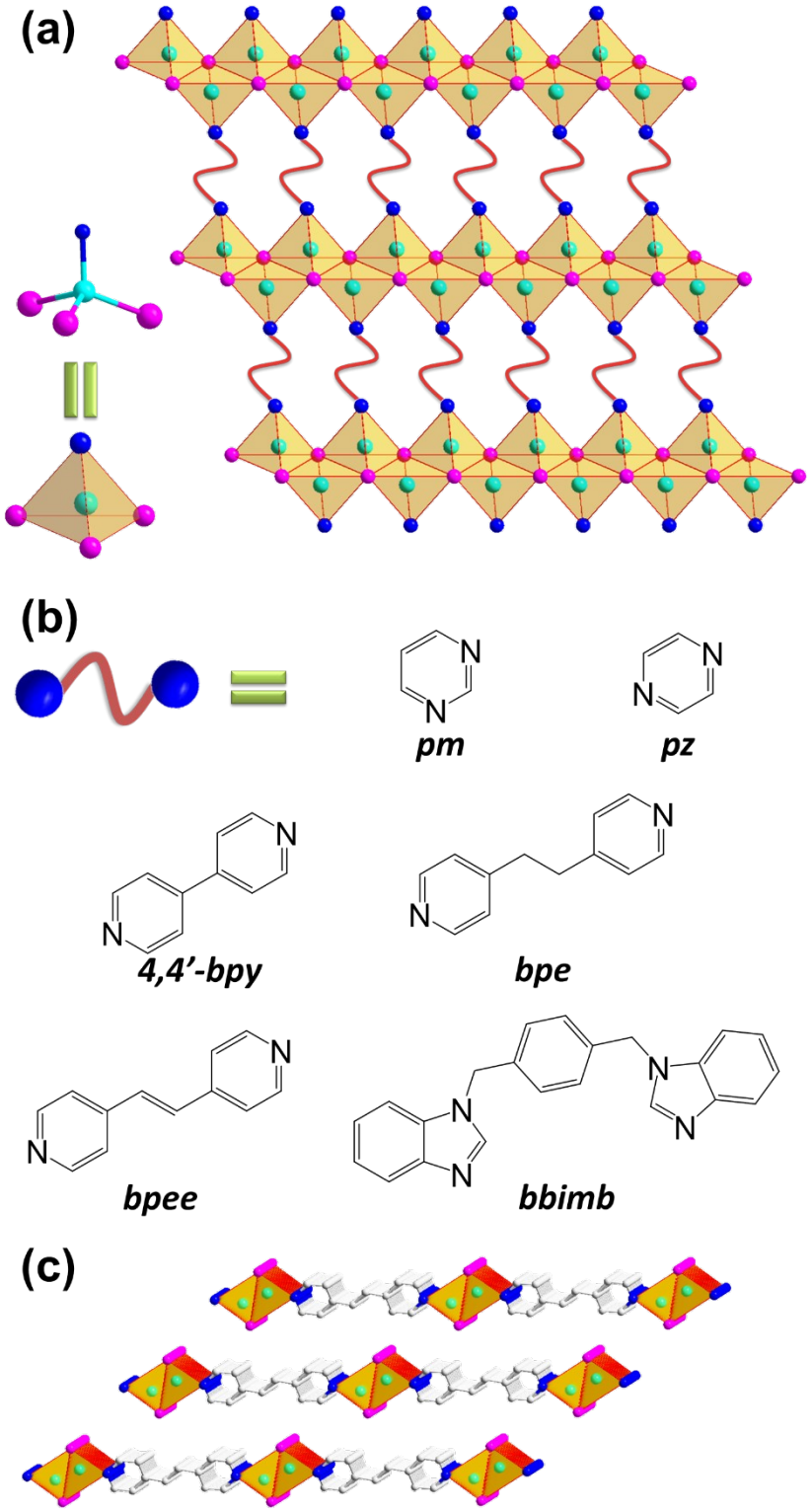

Figure 1. (a) Polyhedral representation of 2D $CuI(L)_{0.5}$. The 1D-CuI chains are connected by bidentate ligands. (b) Bidentate ligands used in this work. (c) View of

2D-CuI(*bpe*)$_{0.5}$ illustrating the staggered arrangement of adjacent sheets. (Cu: cyan, I: pink, N: blue, grey: C).

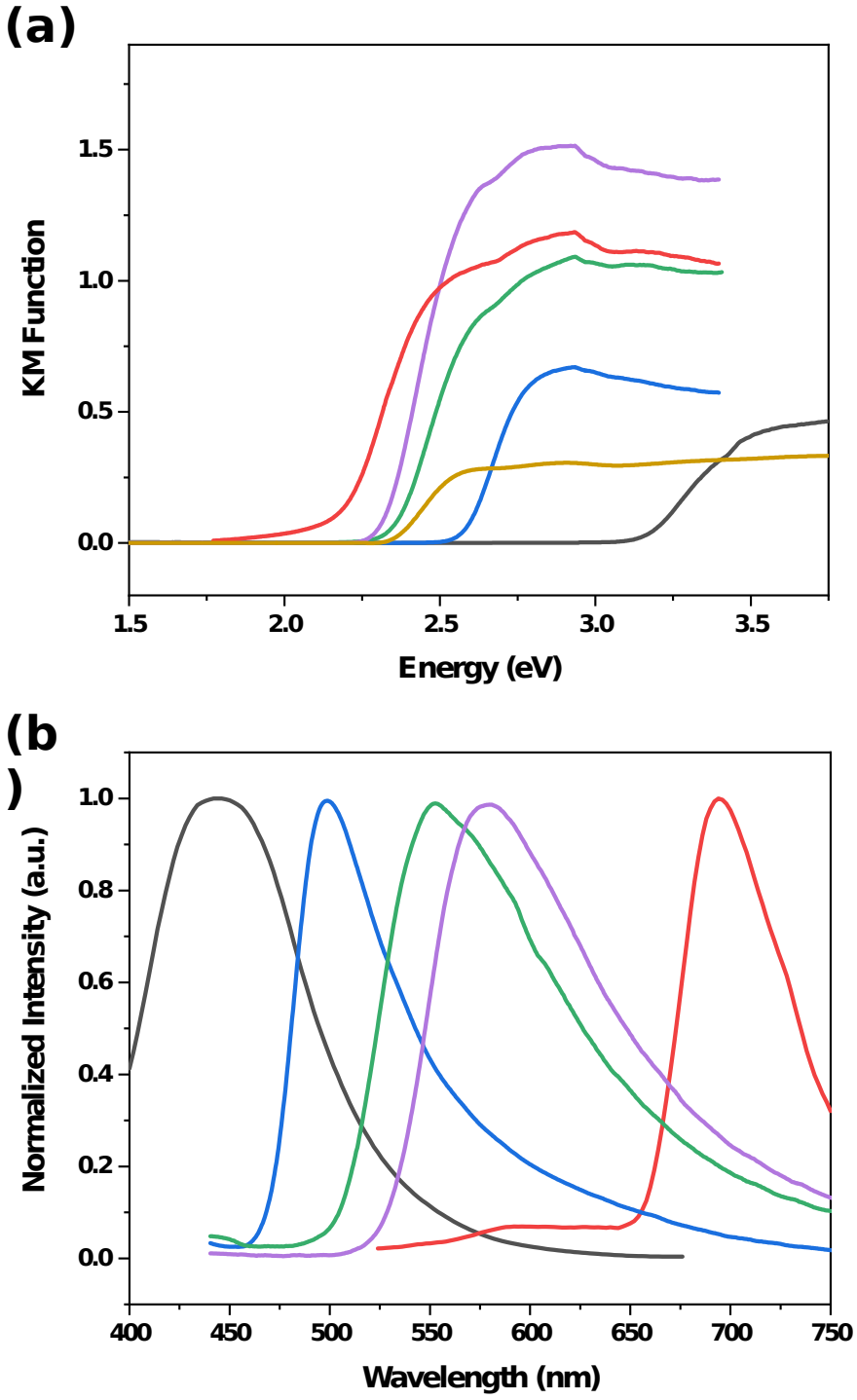

Figure 2. (a) Absorption spectra of **1** (blue), **2** (purple), **3** (green), **4** (black), **5** (red) and **6** (yellow). The steps near 3.4 eV in (a) were caused by the detector changing

of the instrument. (b) photoluminescence spectra of **1** (blue), **2** (purple), **3** (green), **4** (black) and **5** (red). λ_{ex} = 360 nm.

Table 3. Estimated band gaps, emission energies and colors and decomposition temperatures (λ_{ex} = 360 nm)

#	Compound	BG (eV)	λ_{em} (nm)	Emission Color	IQY (%)	Crystal Shape	Crystal Size(mm)	T_D (°C)
1	2D-CuI(*pm*)$_{0.5}$	2.5	500	Green	17.0	Plate	~2	160
2	2D-CuI(*pz*)$_{0.5}$	2.25	578	Yellow	12.7	Plate	~1	170
3	2D-CuI(4,4'-*bpy*)$_{0.5}$	2.3	556	Yellow	2.5	Cubic	~0.3	290
4	2D-CuI(*bpe*)$_{0.5}$	3.1	443	Purple	16.4	Needle	~0.2	280
5	2D-CuI(*bpee*)$_{0.5}$	2.2	695	Red	1.0	Rod	~2	300
6	2D-CuI(*bbimb*)$_{0.5}$	2.35	-	-	-	Plate	~0.1	310

Thermal Stability Analysis.

The decomposition temperatures of compounds **1**-**6** were determined by the thermogravimetric (TG) analyses and the results are listed in Table 3. Most of them are stable up to 250 °C, much more stable than those of 1D-CuI(*L*) structures, which generally decompose around 100 °C (Fig. 3a). Compound **3** was selected for a series of stability measurements and the results show that it exhibits excellent thermal, chemical and photo stability. After heating in the oven at 180 °C, soaking in water, placing under UV light for a week, the sample still maintains its structure and initial crystallinity based on the PXRD analysis (Fig. 3b). The significantly enhanced stability of these structures is due to the formation of higher dimensionality as well as the use of ligands that form strong Cu-N bonds.[21, 23]

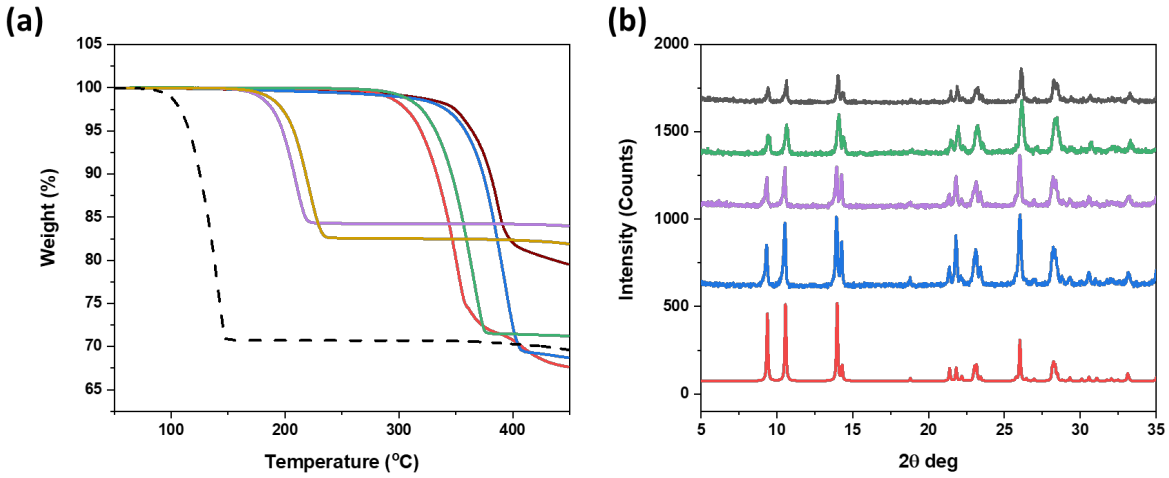

Figure 3. (a) TG plots of **1** (purple), **2** (yellow), **3** (green),**4** (red), **5** (blue) and **6** (brown), in comparison with that of 1D-CuI(*py*) (dashed black). (b) PXRD patterns of compound **3** after various treatments. From bottom to top: simulated (red), as-made (blue), under UV light for a week (purple), soaked in water for a week (green), heated at 180 °C for a week (black).

Electronic Structures.

To understand the electronic structures of these compounds, we performed DFT calculations on selected structures. Generally, their band structures are generally dispersive, suggesting potentially good charge transportation properties. The projected density of states (PDOS) analysis shows that for all compounds, the valance band maximum (VBM) is composed primarily of the atomic orbitals of inorganic motif (i.e., Cu 3*d* and I 5*p* atomic orbitals), whereas the conduction band minimum (CBM) mainly consists of the atomic orbitals of organic ligands (i.e., C 2*p* and N 2*p*), similar to many reported CuX based hybrid materials with (M+X)LCT emission mechanism.[13, 17, 19, 24] (Fig. 4 and Figs. S4-8).

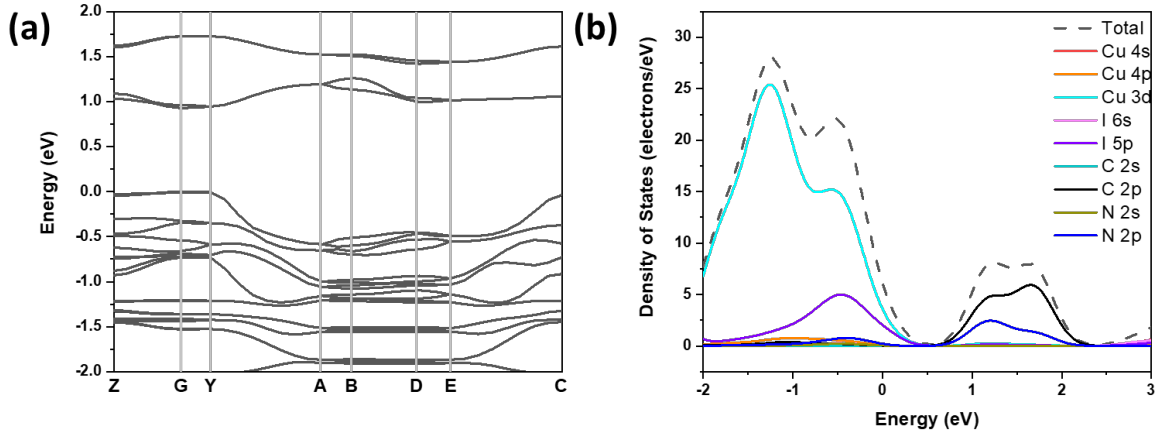

Figure 4. Calculated (a) band sturcture (BS) and (b) projected density of states (PDOS) of compound **1.** The maximum of the valence band is set at 0 eV.

Electric and Transport Properties.

Growing crystals large enough for electric property measurements has always been a challenging task. 2D-CuI(pm)$_{0.5}$ and 2D-CuI(pz)$_{0.5}$ were chosen for electric and transport property studies as they emit at green (λ_{em} = 500 nm) and yellow (λ_{em} = 578 nm) with relatively high quantum yields of 17.0% and 12.7% under 360 nm excitation, respectively (Table 3). Using a modified diffusion growth method, we were able to obtain both compounds with sufficiently large crystals. After a careful screening, two large plate-shaped and *mm*-sized high quality single crystals of CuI(pm)$_{0.5}$ and 2D-CuI(pz)$_{0.5}$ (Fig. 5) were selected for Hall mobility and carrier density measurements.

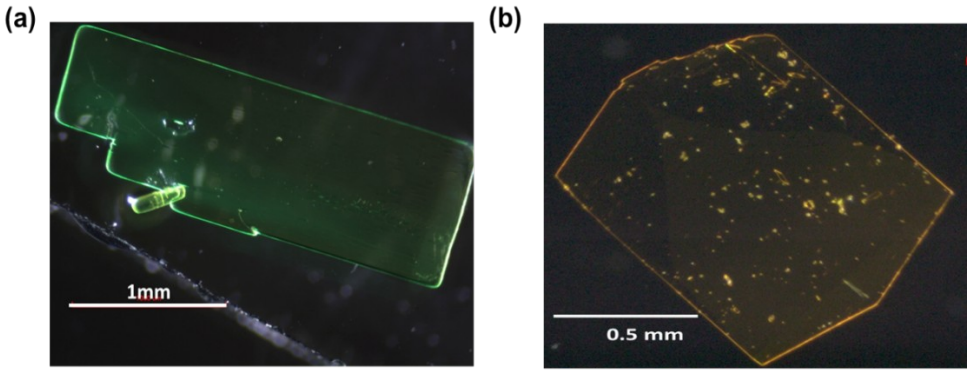

Figure 5. Crystal images of compounds (a) **1** and (b) **2**.

The knowledge of transport parameters, such as intrinsic carrier mobility, dark and photo conductivity and carrier density, are essential for further development of CuI-based hybrid optoelectronic materials and devices. The intrinsic charge transport properties of 2D-CuI(pm)$_{0.5}$ and 2D-CuI(pz)$_{0.5}$ single crystals were investigated by using recently developed highly sensitive *ac* Hall effect measurement technique.[33,34] This method allows for reliable measurements of the intrinsic Hall mobility and carrier density in highly resistive low-μ materials, such as organic semiconductors with carrier mobility as low as μ ~0.1 $cm^2V^{-1}s^{-1}$. It is virtually impossible to resolve Hall effect in such low- μ semiconductors by using conventional dc Hall measurements even in very high magnetic fields (~ 10 T). The novel method uses only a small *ac* magnetic field, rms B = 0.23 T, thus eliminating the need for superconducting magnets and cryogenic equipment necessary in conventional *dc* Hall measurements of high-mobility organic transistors.[35] An *ac* Hall measurement setup used in this study is shown in Fig. 6a.

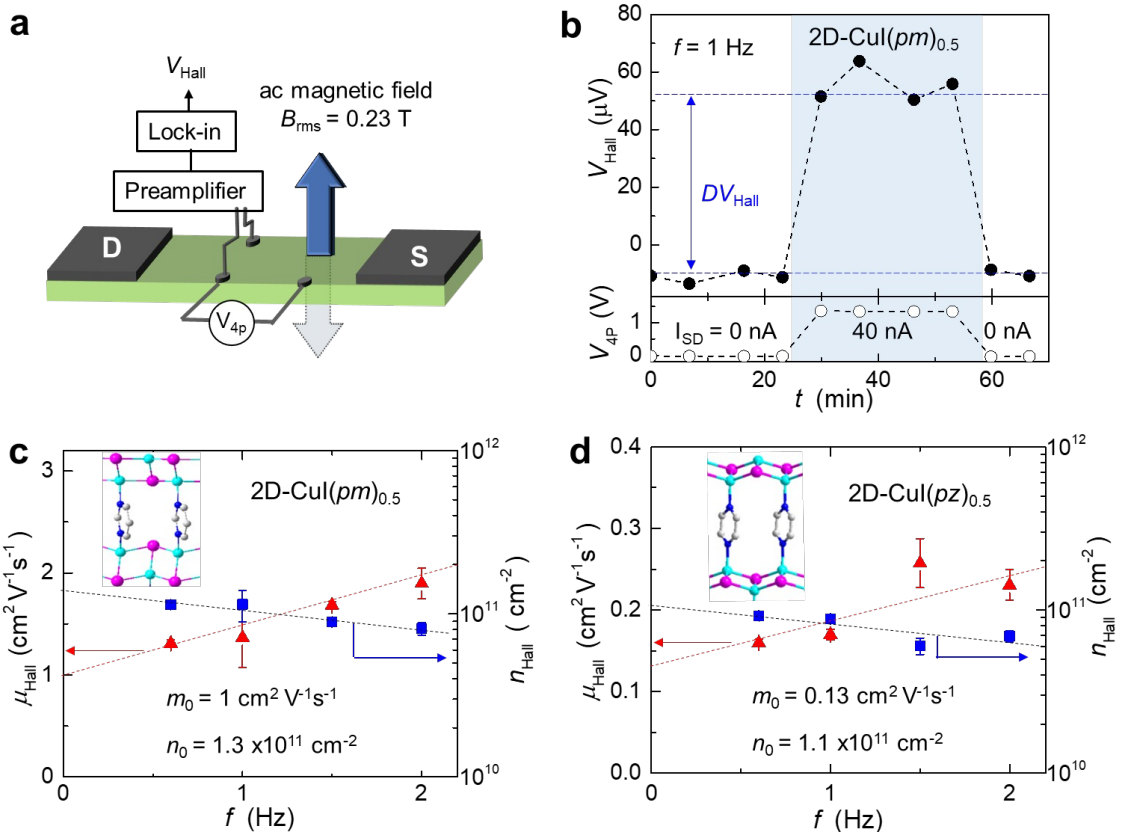

Figure 6. Hall-effect measurement in 2D-CuI-diazine hybrid single crystals. a) Schematics of *ac* Hall-effect measurements. *ac* magnetic field (rms B = 0.23 T) is applied perpendicular to the platelet-like crystal, while a *dc* excitation current is passed through the sample. *dc* four-probe and *ac* Hall voltages are monitored *in-situ*. b) A representative *ac* Hall voltage measured in 2D-CuI(pm)$_{0.5}$ single crystal. The true Hall mobility, μ_0, and carrier density, n_0, are determined by extrapolating $\mu_{Hall}(f)$ and $n_{Hall}(f)$ dependences to zero frequency (f = 0) in order to eliminate the Faraday-induction contribution. c) μ_0 = 1 cm^{2}V^{-1}s^{-1} and n_0 = 1.3×10^{11} cm^{-2} measured in 2D-CuI(pm)$_{0.5}$ single crystal, and d) μ_0 = 0.13 cm^{2}V^{-1}s^{-1} and n_0 = 1.1×10^{11} cm^{-2} measured in 2D-CuI(pz)$_{0.5}$ single crystal.

We drive a *dc* excitation current through the sample in the longitudinal direction, while an *ac* magnetic field B = 0.23 T (with frequency, f = 0.5-2.5 Hz) is applied perpendicular to the flat facet of the crystal, and an *ac* Hall voltage, V_{Hall}, is measured by a lock-in technique in transverse direction across the sample. In order to account for the contact resistance effects, four-probe contact configuration is used, and a longitudinal 4-probe voltage, V_{4P}, is measured along the channel as well. Hall and 4-probe voltages measured in 2D-CuI(pm)$_{0.5}$ single crystal are shown in Fig. 6b. *dc* channel excitation currents, I_{SD} = 0 and 40 nA, are applied intermittently, while V_{Hall} and V_{4P} signals are recorded. The Hall voltage, V_{Hall}, is found from the difference between V_{Hall}(40 nA) and V_{Hall}(0), which allows to account for undesirable Faraday induction (for details, see a reference[33]). Hall mobility,

μ_{Hall}, and carrier density, n_{Hall}, are obtained by using the following equations: $\mu_{Hall} = (D/W) \bullet V_{4P}^{-1} \bullet dV_{Hall}/dB$ and $n_{Hall} = n_{Hall} = I \bullet e^{-1} \bullet (dV_{Hall}/dB)^{-1}$, where D is the distance between the voltage probes along the channel in the four-probe contact geometry, and W is the channel width. The true Hall mobility, μ_0, is determined by taking these measurements at several frequencies and extrapolating $\mu_{Hall}(f)$ to zero frequency, $f = 0$, which further helps to eliminate an unwanted Faraday induction. True carrier density, n_0, is also determined by extrapolation to $f = 0$. The resultant Hall mobilities (carrier densities) are $\mu_0 = 1$ $cm^2V^{-1}s^{-1}$ ($n_0 = 1.3\times10^{11}$ cm^{-2}) and 0.13 $cm^2V^{-1}s^{-1}$ ($n_0 = 1.1\times10^{11}$ cm^{-2}) in 2D-CuI$(pm)_{0.5}$ and 2D-CuI$(pz)_{0.5}$ single crystals, respectively, as shown in Figs. 6c and 6d.

The observed carrier mobilities in 2D-CuI$(pm)_{0.5}$ and 2D-CuI$(pz)_{0.5}$ single crystals are over 4 orders of magnitude higher than those in the typical strongly emissive organic semiconductors (10^{-6} - 10^{-5} $cm^2V^{-1}s^{-1}$).[3,4, 36,37] Given the outstanding carrier mobility of these hybrids, as compared to that of known luminescent organic semiconductors, we believe that these materials are promising for development of novel optical devices, such as light-emitting transistors.[38-39]

We also performed Scanning Kelvin Probe Microscope (SKPM) in electrostatic force microscope mode of AFM instrument (Park Systems NX-10) to determine the work function of 2D-CuI$(pm)_{0.5}$ and 2D-CuI$(pz)_{0.5}$ in order to make anode and cathode contacts for a single crystal device application. SKPM provided the electrical potential mapping at room temperature in air. We extracted both work functions from the contact potential difference between the sample surface and the AFM/SKPM tip. The highly oriented pyrolytic graphite (HOPG) is used as a reference, which is stable in air with work function of 5.5 eV obtained from ultraviolet photoelectron spectroscopy (UPS). The average potential differences of the 2D-CuI$(pm)_{0.5}$ and 2D-CuI$(pz)_{0.5}$ are -34 mV and -240 mV, respectively, resulting in the work functions of 5.46 eV and 5.26 eV respectively. 2D-CuI$(pm)_{0.5}$ displays valance band maximum (VBM)/conduction band minimum (CBM) levels of -5.4/-2.9 eV estimated from SKPM and optical band gap. Fig. 7 shows energy levels and effectively injection of electron and hole into the hybrid crystals.

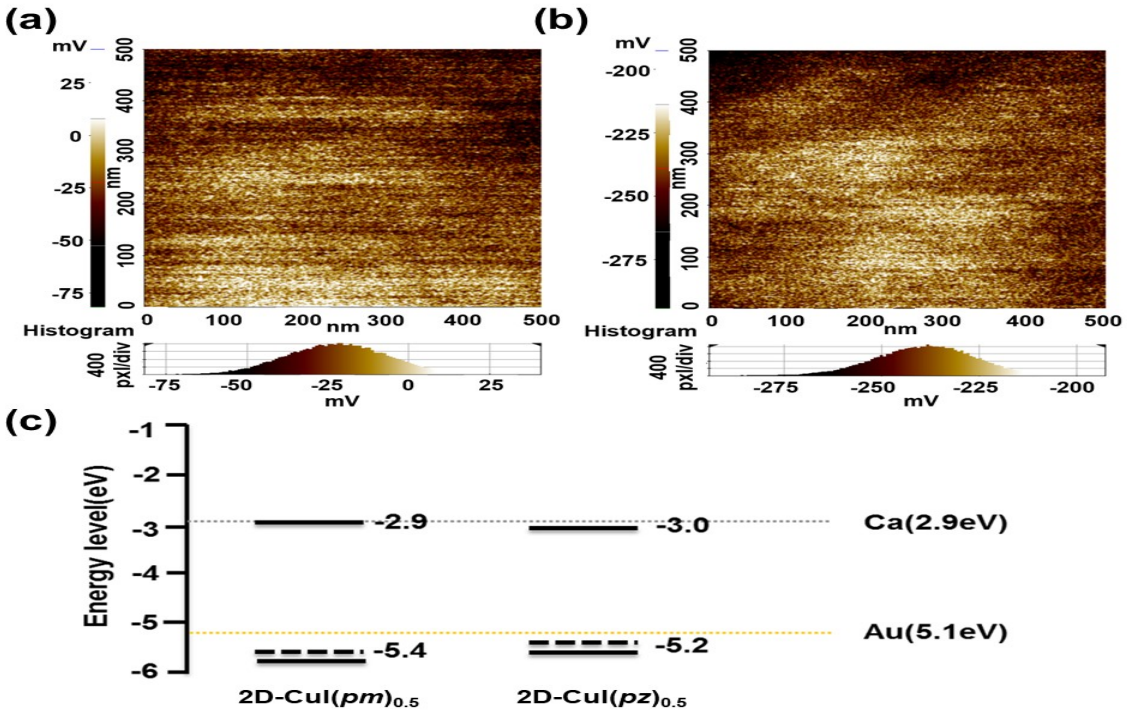

Figure 7. Surface potential map of (a) 2D-CuI(pm)$_{0.5}$ and (b) 2D-CuI(pz)$_{0.5}$ by SKPM in air. The relatively uniform surface potential was shown in both samples. (c) Schematic energy band diagrams of 2D-CuI(pm)$_{0.5}$ and 2D-CuI(pz)$_{0.5}$ measured by Kelvin Probe microscope measurement.

Conclusions

A group of two-dimensional 2D-CuI(L)$_{0.5}$ structures have been synthesized and structurally characterized. These compounds exhibit systematic electronic and optical tunability similar to several other types of CuI-based hybrid semiconductor materials, including 0D-Cu_2I_2(L) dimer-based and 1D-CuI(L) chain-based structures.[17-19, 24, 40] They possess significantly improved stability as a result of increased framework dimensionality and enhanced Cu-N bonding. Their electronic structures were analyzed by DFT calculations, and their electric and transport property measurements were carried out on high quality, large single crystals of 2D-CuI(pm)$_{0.5}$ and 2D-CuI(pz)$_{0.5}$. The

results show that both compounds display p-type conductivity in the dark, with a Hall mobility and charge density of ~1$cm^2V^{-1}s^{-1}$ and 1.3×10^{11} cm^{-2} for 2D-CuI(*pm*)$_{0.5}$, and 0.13 $cm^2V^{-1}s^{-1}$ and 1.1×10^{11} cm^{-2} for 2D-CuI(*pz*)$_{0.5}$, respectively. These values are considerably higher compared to motilities of typical highly luminescent organic semiconductors. This study demonstrates that copper iodide hybrid materials are promising for future applications in light emitting devices.

Supporting Information

Structure plots, PXRD patterns, PL spectra, and DFT calculation results are included in the Supporting Information and this material is available free of charge via the Internet at http://pubs.acs.org.

Acknowledgment

Financial support from the Materials Sciences and Engineering Division, Office of Basic Research Energy Sciences of the U.S. Department of Energy through Grant No. DE-SC0019902 is gratefully acknowledged. The Advanced Light Source (ALS) was supported by the Director, Office of Science, Office of Basic Energy Science, of the U.S. Department of Energy, under contract DE-AC02-05CH11231. We would like to thank Dr. Hai-Lun Xia for helping with the design of cover art image.

References

1. Uoyama, H.; Goushi, K.; Shizu, K.; Nomura, H.; Adachi, C., Highly efficient organic light-emitting diodes from delayed fluorescence. *Nature* **2012,** *492* (7428), 234-+.
2. Zhu, X. H.; Peng, J. B.; Caoa, Y.; Roncali, J., Solution-processable single-material molecular emitters for organic light-emitting devices. *Chem Soc Rev* **2011,** *40* (7), 3509-3524.
3. Geens, W.; Shaheen, S. E.; Wessling, B.; Brabec, C. J.; Poortmans, J.; Serdar Sariciftci, N., Dependence of field-effect hole mobility of PPV-based polymer films on the spin-casting solvent. *Org. Electron.* **2002,** *3* (3–4), 105-110.
4. Yersin, H.; Finkenzeller, W. J.; Walter, M. J.; Djurovich, P. I.; Thompson, M. E., Highly Efficient OLEDs with Phosphorescent Materials. *1st ed.; Wiley-VCH: Weinheim, Germany, 2008; p 458.*
5. Jurchescu, O. D.; Baas, J.; Palstra, T. T. M., Effect of impurities on the mobility of single crystal pentacene. *App. Phys. Lett.* **2004,** *84* (16), 3061-3063.
6. Sundar, V. C.; Zaumseil, J.; Podzorov, V.; Menard, E.; Willett, R. L.; Someya, T.; Gershenson, M. E.; Rogers, J. A., Elastomeric Transistor Stamps: Reversible Probing of Charge Transport in Organic Crystals. *Science* **2004,** *303* (5664), 1644-1646.

7. Najafov, H.; Lee, B.; Zhou, Q.; Feldman, L. C.; Podzorov, V., Observation of long-range exciton diffusion in highly ordered organic semiconductors. *Nat. Mater.* **2010,** *9* (11), 938-943.
8. Cai, M.; Xiao, T.; Hellerich, E.; Chen, Y.; Shinar, R.; Shinar, J., High-Efficiency Solution-Processed Small Molecule Electrophosphorescent Organic Light-Emitting Diodes. *Adv. Mater.* **2011,** *23* (31), 3590-3596.
9. Zhang, X.; Sun, R.; Zheng, Q.; Kobayashi, T.; Li, W., Temperature-dependent electroluminescence from (Eu, Gd) coordination complexes. *Appl. Phys. Lett.* **1997,** *71* (18), 2596-2598.
10. Baldo, M. A.; Kozlov, V. G.; Burrows, P. E.; Forrest, S. R.; Ban, V. S.; Koene, B.; Thompson, M. E., Low pressure organic vapor phase deposition of small molecular weight organic light emitting device structures. *Appl. Phys. Lett.* **1997,** *71* (21), 3033-3035.
11. Tang, C. W.; VanSlyke, S. A., Organic electroluminescent diodes. *Appl. Phys. Lett.* **1987,** *51* (12), 913-915.
12. Liu, W.; Zhu, K.; Teat, S. J.; Deibert, B. J.; Yuan, W.; Li, J., A mechanochemical route toward the rational, systematic, and cost-effective green synthesis of strongly luminescent copper iodide based hybrid phosphors. *J. Mater. Chem. C* **2017,** *5* (24), 5962-5969.
13. Liu, W.; Zhu, K.; Teat, S. J.; Dey, G.; Shen, Z.; Wang, L.; O'Carroll, D. M.; Li, J., All-in-One: Achieving Robust, Strongly Luminescent and Highly Dispersible Hybrid Materials by Combining Ionic and Coordinate Bonds in Molecular Crystals. *J. Am. Chem. Soc.* **2017,** *139* (27), 9281-9290.
14. Fang, Y.; Liu, W.; Teat, S. J.; Dey, G.; Shen, Z.; An, L.; Yu, D.; Wang, L.; O'Carroll, D. M.; Li, J., A Systematic Approach to Achieving High Performance Hybrid Lighting Phosphors with Excellent Thermal- and Photostability. *Adv. Funct. Mater.* **2017,** *27* (3), 1603444.
15. Liu, W.; Fang, Y.; Wei, G. Z.; Teat, S. J.; Xiong, K.; Hu, Z.; Lustig, W. P.; Li, J., A Family of Highly Efficient CuI-Based Lighting Phosphors Prepared by a Systematic, Bottom-up Synthetic Approach. *J. Am. Chem. Soc.* **2015,** *137* (29), 9400-9408.
16. Liu, W.; Lustig, W. P.; Li, J., Luminescent inorganic-organic hybrid semiconductor materials for energy-saving lighting applications. *EnergyChem* **2019,** *1* (2), 100008.
17. Fang, Y.; Sojdak, C. A.; Dey, G.; Teat, S. J.; Li, M.; Cotlet, M.; Zhu, K.; Liu, W.; Wang, L.; ÓCarroll, D. M.; Li, J., Highly efficient and very robust blue-excitable yellow phosphors built on multiple-stranded one-dimensional inorganic–organic hybrid chains. *Chem. Sci.* **2019,** *10* (20), 5363-5372.
18. Hei, X.; Teat, S. J.; Liu, W.; Li, J., Eco-friendly, solution-processable and efficient low-energy lighting phosphors: copper halide based hybrid semiconductors Cu4X6(L)2 (X = Br, I) composed of covalent, ionic and coordinate bonds. *J. Mater. Chem. C* **2020,** *8* (47), 16790-16797.
19. Hei, X.; Liu, W.; Zhu, K.; Teat, S. J.; Jensen, S.; Li, M.; O'Carroll, D. M.; Wei, K.; Tan, K.; Cotlet, M.; Thonhauser, T.; Li, J., Blending Ionic and Coordinate Bonds in Hybrid Semiconductor Materials: A General Approach

toward Robust and Solution-Processable Covalent/Coordinate Network Structures. *J. Am. Chem. Soc.* **2020,** *142* (9), 4242-4253.
20. Artem'ev, A. V.; Davydova, M. P.; Hei, X.; Rakhmanova, M. I.; Samsonenko, D. G.; Bagryanskaya, I. Y.; Brylev, K. A.; Fedin, V. P.; Chen, J.-S.; Cotlet, M.; Li, J., Family of Robust and Strongly Luminescent CuI-Based Hybrid Networks Made of Ionic and Dative Bonds. *Chem. Mater.* **2020,** *32* (24), 10708-10718.
21. Hei, X.; Li, J., All-in-one: a new approach toward robust and solution-processable copper halide hybrid semiconductors by integrating covalent, coordinate and ionic bonds in their structures. *Chem. Sci.* **2021,** *12* (11), 3805-3817.
22. Peng, R.; Li, M.; Li, D., Copper(I) halides: A versatile family in coordination chemistry and crystal engineering. *Coord. Chem. Rev.* **2010,** *254* (1–2), 1-18.
23. Wei, L.; Yang, F.; Jing, L., Copper Iodide Based Hybrid Phosphors for Energy-Efficient General Lighting Technologies. *Adv. Funct. Mater.* **2018,** *28* (8), 1705593.
24. Zhang, X.; Liu, W.; Wei, G. Z.; Banerjee, D.; Hu, Z.; Li, J., Systematic Approach in Designing Rare-Earth-Free Hybrid Semiconductor Phosphors for General Lighting Applications. *J. Am. Chem. Soc.* **2014,** *136* (40), 14230-14236.
25. Jess, I.; Taborsky, P.; Pospisil, J.; Nather, C., Synthesis, crystal structure, thermal and luminescence properties of CuX(2,3-dimethylpyrazine) (X=Cl, Br, I) coordination polymers. *Dalton Trans* **2007,** (22), 2263-70.
26. Näther, C.; Greve, J.; Jeß, I., Synthesis, crystal structures and thermal properties of new copper(I) halide coordination polymers. *Solid State Sci.* **2002,** *4* (6), 813-820.
27. Conesa-Egea, J.; Redondo, C. D.; Martínez, J. I.; Gómez-García, C. J.; Castillo, Ó.; Zamora, F.; Amo-Ochoa, P., Supramolecular Interactions Modulating Electrical Conductivity and Nanoprocessing of Copper–Iodine Double-Chain Coordination Polymers. *Inorg. Chem.* **2018,** *57* (13), 7568-7577.
28. Hassanein, K.; Conesa-Egea, J.; Delgado, S.; Castillo, O.; Benmansour, S.; Martínez, J. I.; Abellán, G.; Gómez-García, C. J.; Zamora, F.; Amo-Ochoa, P., Electrical Conductivity and Strong Luminescence in Copper Iodide Double Chains with Isonicotinato Derivatives. *Chem. Eur. J.* **2015,** *21* (48), 17282-17292.
29. Blake, A. J.; Brooks, N. R.; Champness, N. R.; Cooke, P. A.; Crew, M.; Deveson, A. M.; Hanton, L. R.; Hubberstey, P.; Fenske, D.; Schröder, M., Copper(I) iodide coordination networks–controlling the placement of $(CuI)_\infty$ ladders and chains within two-dimensional sheets. *Cryst. eng.* **1999,** *2* (2–3), 181-195.
30. Bril, A.; De Jager-Veenis, A. W., *J. Electrochem. Soc.* **1976,** *123*, 396.
31. Bai, X.; Caputo, G.; Hao, Z.; Freitas, V. T.; Zhang, J.; Longo, R. L.; Malta, O. L.; Ferreira, R. A. S.; Pinna, N., Efficient and tuneable photoluminescent

boehmite hybrid nanoplates lacking metal activator centres for single-phase white LEDs. *Nat Commun* **2014,** *5*.
32. Janiak, C., A critical account on π–π stacking in metal complexes with aromatic nitrogen-containing ligands. *Journal of the Chemical Society, Dalton Transactions* **2000,** (21), 3885-3896.
33. Chen, Y.; Yi, H. T.; Podzorov, V., High-Resolution ac Measurements of the Hall Effect in Organic Field-Effect Transistors. *Phys. Rev. Applied* **2016,** *5* (3), 034008.
34. Yi, H. T.; Gartstein, Y. N.; Podzorov, V., Charge carrier coherence and Hall effect in organic semiconductors. *Sci. Rep.* **2016,** *6*, 23650.
35. Podzorov, V.; Menard, E.; Rogers, J. A.; Gershenson, M. E., Hall Effect in the Accumulation Layers on the Surface of Organic Semiconductors. *Phys. Rev. Lett.* **2005,** *95* (22), 226601.
36. Ma, D.; Wang, G.; Hu, Y.; Zhang, Y.; Wang, L.; Jing, X.; Wang, F.; Lee, C. S.; Lee, S. T., A dinuclear aluminum 8-hydroxyquinoline complex with high electron mobility for organic light-emitting diodes. *Appl. Phys. Lett.* **2003,** *82* (8), 1296-1298.
37. Assadi, A.; Svensson, C.; Willander, M.; Inganäs, O., Field-effect mobility of poly(3-hexylthiophene). *Appl. Phys. Lett.* **1988,** *53* (3), 195-197.
38. Capelli, R.; Toffanin, S.; Generali, G.; Usta, H.; Facchetti, A.; Muccini, M., Organic light-emitting transistors with an efficiency that outperforms the equivalent light-emitting diodes. *Nat. Mater.* **2010,** *9* (6), 496-503.
39. Zaumseil, J.; Friend, R. H.; Sirringhaus, H., Spatial control of the recombination zone in an ambipolar light-emitting organic transistor. *Nat. Mater.* **2006,** *5* (1), 69-74.
40. Liu, W.; Fang, Y.; Wei, G. Z.; Teat, S. J.; Xiong, K.; Hu, Z.; Lustig, W. P.; Li, J., A Family of Highly Efficient CuI-Based Lighting Phosphors Prepared by a Systematic, Bottom-up Synthetic Approach. *J. Am. Chem. Soc.* **2015,** *137* (29), 9400-9408.